NANO EXPRESS

Open Access

CrossMark

Analysis on the Filament Structure Evolution in Reset Transition of Cu/HfO$_2$/Pt RRAM Device

Meiyun Zhang[1,2], Shibing Long[1,2]*, Yang Li[1,2], Qi Liu[1,2], Hangbing Lv[1,2], Enrique Miranda[3], Jordi Suñé[3] and Ming Liu[1,2]

Abstract

The resistive switching (RS) process of resistive random access memory (RRAM) is dynamically correlated with the evolution process of conductive path or conductive filament (CF) during its breakdown (rupture) and recovery (reformation). In this study, a statistical evaluation method is developed to analyze the filament structure evolution process in the reset operation of Cu/HfO$_2$/Pt RRAM device. This method is based on a specific functional relationship between the Weibull slopes of reset parameters' distributions and the CF resistance (R_{on}). The CF of the Cu/HfO$_2$/Pt device is demonstrated to be ruptured abruptly, and the CF structure of the device has completely degraded in the reset point. Since no intermediate states are generated in the abrupt reset process, it is quite favorable for the reliable and stable one-bit operation in RRAM device. Finally, on the basis of the cell-based analytical thermal dissolution model, a Monte Carlo (MC) simulation is implemented to further verify the experimental results. This work provides inspiration for RRAM reliability and performance design to put RRAM into practical application.

Keywords: RRAM, Conductive filament (CF), Structure evolution, Monte Carlo simulator

Background

With conventional flash memories approaching their technical and physical limits, there will be severe problems in the scaling of solid-state memory [1–4]. A great amount of research attention has been focused on the next generation memory devices. Resistive random access memory (RRAM), with the reversible and reproducible resistive switching (RS) phenomena induced by applied electric field has been extensively studied due to its potential applications in high density memory [5] and neuromorphic electronic systems [6–9]. The electrochemical metallization (ECM)-based RRAM with an active metal electrode such as Ag or Cu is referred to as programmable metallization cell (PMC) or conductive bridge RAM (CBRAM), which is an important type of RRAM device. The RS phenomena of the PMC are attributed to the oxidation of the active anode metal into cations, the transport of these cations, and their reduction on the cathode or in the RS layer [10–12]. Via the above redox process, the nanoscale conductive filaments (CFs) are formed in the set process and ruptured in the reset process in the RS layer [13–21]. The confinement of the resistive switching phenomenon to a nanometric filament has been widely demonstrated by conductive AFM [22–24] and cross-sectional TEM [25, 26]. However, the filamentary switching has the stochastic nature, similar to the dielectric breakdown, which has ever been a serious obstacle to boost RRAM into practical applications [27–30]. Studying the statistics of the RS parameters [31, 32] is also significant to discover the filament annihilation/reconstruction information and guide us to improve the uniformity. The Weibull distribution has been often used to analyze the statistics of electron devices. Because the initial filament width or on-state resistance (R_{on})

* Correspondence: longshibing@ime.ac.cn
[1]Key Laboratory of Microelectronics Devices and Integrated Technology, Institute of Microelectronics of Chinese Academy of Sciences, Beijing 100029, China
[2]Jiangsu National Synergetic Innovation Center for Advanced Materials (SICAM), Nanjing 210023, China
Full list of author information is available at the end of the article

Zhang *et al. Nanoscale Research Letters* (2016) 11:269

Page 2 of 6

has a significant impact on the reset transition process and there is an analytical correlationship between the Weibull slopes (β) of reset parameters' distributions and CF size or R_{on} [33, 34], this relationship could be made use of to analyze the filament microstructure evolution. At the reset point where the current is the maximum in the reset I–V curve, when β the Weibull slope changes with R_{on}, the degradation of the CF structure has occurred, and the reset transition inclines to be abrupt [33]. On the contrary, the CF just starts to dissolve at the reset point and the reset switching tends to be gradual [34] when β the Weibull slope is a constant, independent on R_{on}.

In this paper, the annihilation behavior of the filament in Cu/HfO$_2$/Pt PMC device is investigated according to the above mentioned statistical evaluation method. The Weibull slopes (β_V and β_I) of our Cu/HfO$_2$/Pt CBRAM device decrease with R_{on}, so the filament dissolution or the reset transition is abrupt. A Monte Carlo method is utilized to simulate and capture the experimental results. The controllable abrupt reset operation will bring great benefits to the reliable binary operation of RRAM. Our work has great significance in providing inspiration for RRAM performance and reliability design to put RRAM into practical application.
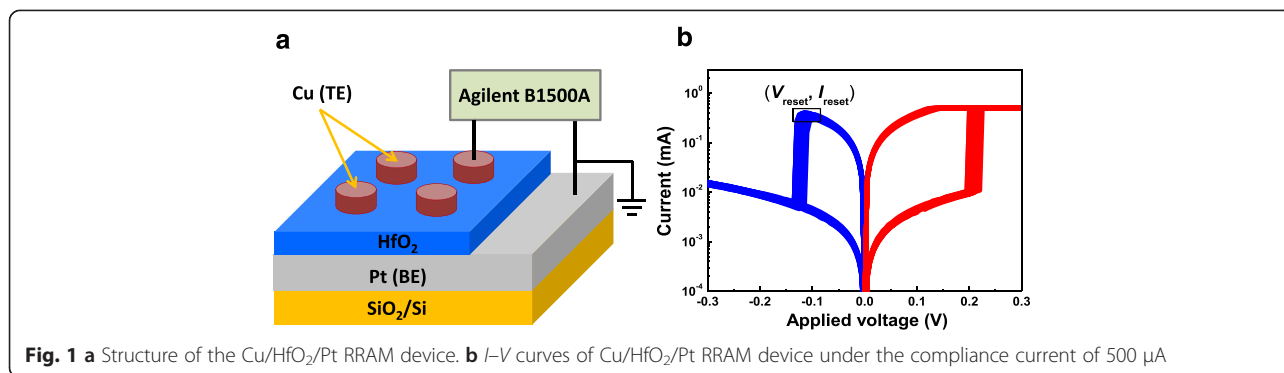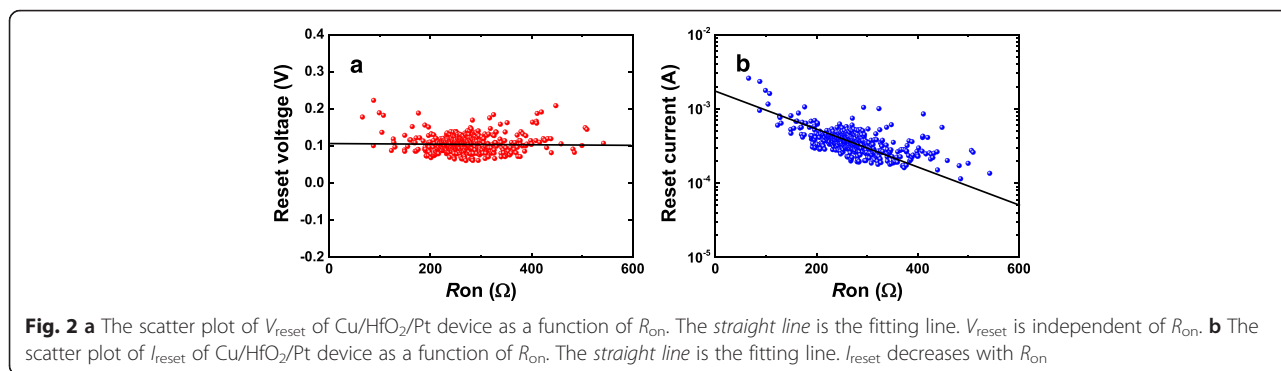
Methods

The Cu/HfO$_2$/Pt device with the schematic structure shown in Fig. 1a is comprised of an inert Pt bottom electrode (BE), a HfO$_2$ RS layer, and an oxidizable Cu metal top electrode (TE). A 20-nm-thick Pt BE and a 10-nm-thick HfO$_2$ layer were sequentially deposited by magnetron sputtering on SiO$_2$/Si substrate. Then, Cu TE was sputtered and patterned to have a thickness of 40 nm and an area of 100×100 μm^2. The electrical characteristics of the device were measured by Agilent B1500A semiconductor device parameter analyzer. The I–V curves were tested under the DC voltage sweep mode, where the bias voltage was applied to the TE with the BE grounded. Figure 1b shows the 20 I–V curves of the Cu/HfO$_2$/Pt device.

Results and Discussion

Figure 1b shows 20 I–V curves of the Cu/HfO$_2$/Pt device. We can find that these curves present abrupt switching during set and reset cycles. The reset points are defined as those having and are the maximum current in the I–V curves in reset process, and their voltages and currents are defined as V_{reset} and I_{reset}, respectively. To investigate whether the degradation of CF microstructure has occurred or not before the reset point, 1000 continuous set/reset cycles have been measured to get the V_{reset} and I_{reset} statistical characteristics. Figure 2 presents the scatter plots for V_{reset} and I_{reset} dependent on R_{on}. V_{reset} keeps constant and I_{reset} decreases with R_{on}. We can find that R_{on} has influence on some parameters of V_{reset} and I_{reset} distributions.

To study the correlation of V_{reset} and I_{reset} with R_{on} in detail, the whole R_{on} range was divided into several ranges using the screening method [33, 34]. The method of the separation of the data into different groups does not influence the final statistical results, i.e., the results keep a certain regularity regardless of the different grouping methods. Weibull distribution is used to describe the distributions of V_{reset} and I_{reset} in each range. Figure 3a, b shows the Weibull distributions of V_{reset} and I_{reset} in grouped R_{on} range, respectively. We can find that the distributions in each range have some tails. However, these tails just occupy a little proportion of the overall distribution in each range, which does not affect the global tendency of the distribution. Through the linear fittings to experimental V_{reset} and I_{reset} distributions in different groups, we can obtain the Weibull slopes (β_V and β_I) and scale factors ($V_{reset63\%}$ and $I_{reset63\%}$). Figure 3c, d shows that β_V and β_I Weibull slopes are linear to $1/R_{on}$, while $V_{reset63\%}$ the scale factor is constant and $I_{reset63\%}$ is linear to $1/R_{on}$. The experimental results can be explained by the cell-based thermal dissolution model [33] with its geometric model shown in Fig. 4. According to this model, the reset is determined by the narrowest part of the filament consisting of N slices of cells with each slice including n cells. When at least one slice of cells is "defective" under thermal dissolution mechanism, e.g., the oxygen vacancies

Fig. 1 a Structure of the Cu/HfO$_2$/Pt RRAM device. **b** I–V curves of Cu/HfO$_2$/Pt RRAM device under the compliance current of 500 μA

Zhang *et al. Nanoscale Research Letters* (2016) 11:269

Page 3 of 6

Fig. 2 a The scatter plot of V_{reset} of Cu/HfO$_2$/Pt device as a function of R_{on}. The *straight line* is the fitting line. V_{reset} is independent of R_{on}. **b** The scatter plot of I_{reset} of Cu/HfO$_2$/Pt device as a function of R_{on}. The *straight line* is the fitting line. I_{reset} decreases with R_{on}
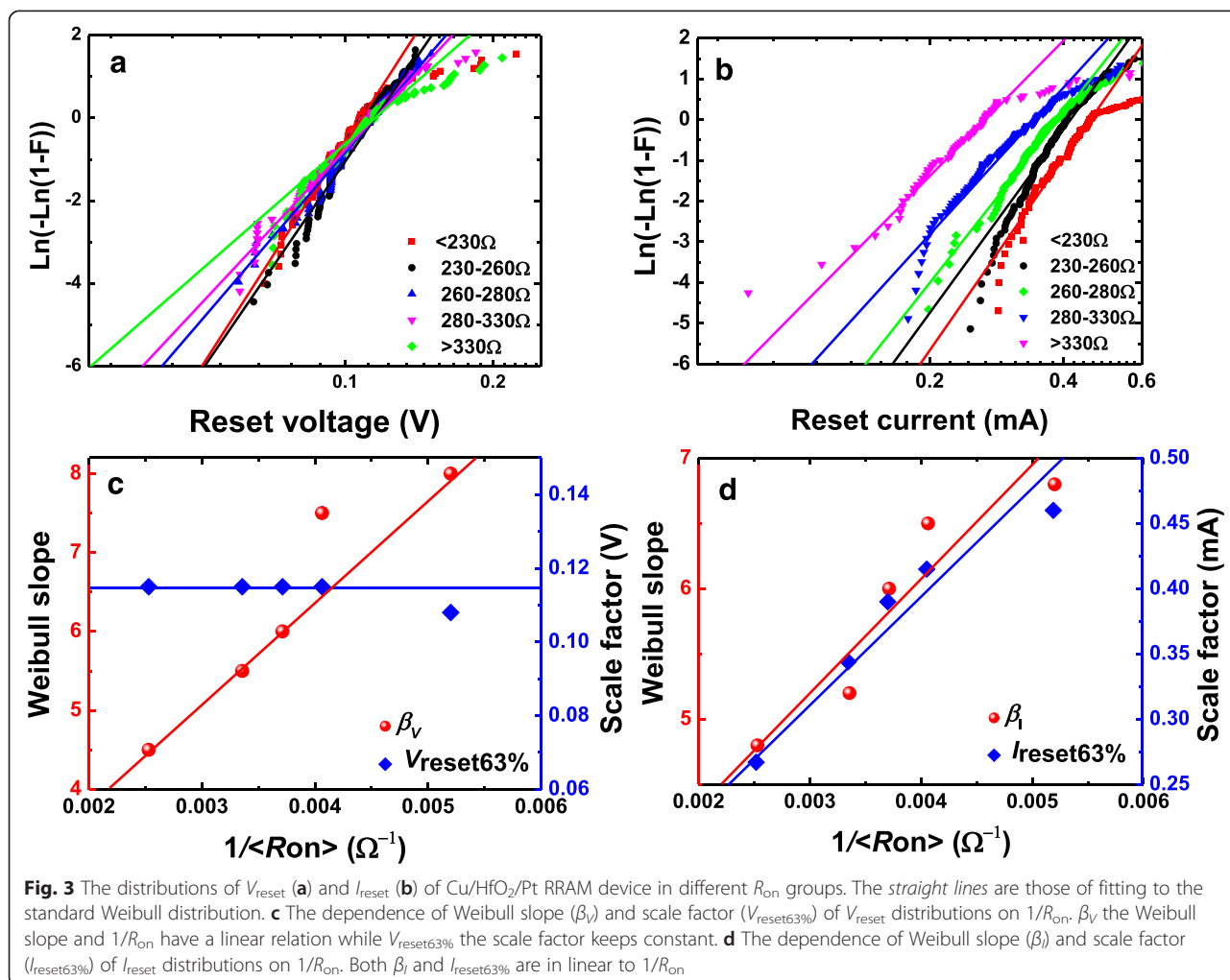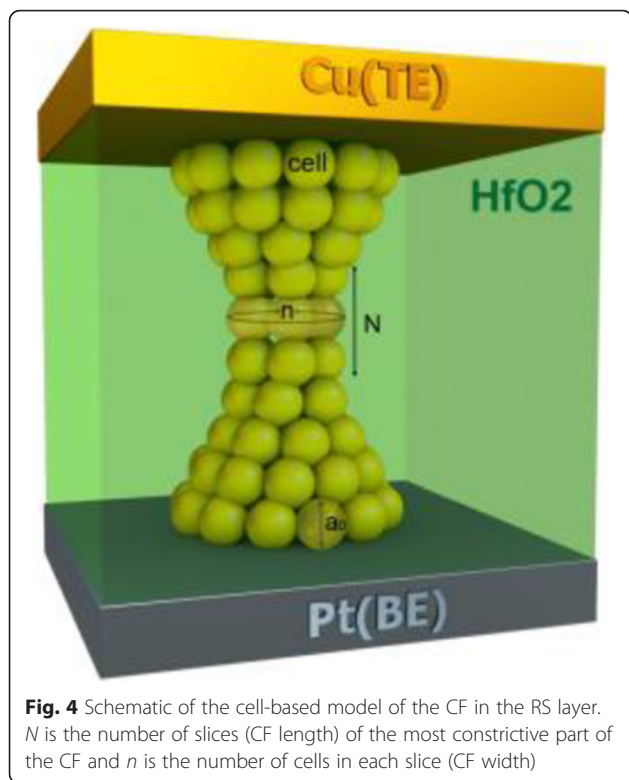
are occupied by oxygen ions, the reset transition occurs. In Ref. [33], the cell model was constructed for unipolar valence change mechanism (VCM) device in which the reset transition is dominated by the thermal dissolution of CF. Here we find that the cell model is also suitable for the experimental statistics of oxide-based ECM device in this work. The reset of this kind of ECM device can be understood as that the metal atoms (Cu) in CF are

oxidized into cations and diffuse out from the CF region under the Joule heat generated in CF. The most important result of the cell model is that the Weibull slopes of V_{reset} and I_{reset} distribution are linearly dependent on the CF size, i.e., $1/R_{on}$, which is expressed by:

$$\beta_V = \beta_I = kn, \tag{1}$$

Fig. 3 The distributions of V_{reset} (**a**) and I_{reset} (**b**) of Cu/HfO$_2$/Pt RRAM device in different R_{on} groups. The *straight lines* are those of fitting to the standard Weibull distribution. **c** The dependence of Weibull slope (β_V) and scale factor ($V_{reset63\%}$) of V_{reset} distributions on $1/R_{on}$. β_V the Weibull slope and $1/R_{on}$ have a linear relation while $V_{reset63\%}$ the scale factor keeps constant. **d** The dependence of Weibull slope (β_I) and scale factor ($I_{reset63\%}$) of I_{reset} distributions on $1/R_{on}$. Both β_I and $I_{reset63\%}$ are in linear to $1/R_{on}$

Zhang *et al. Nanoscale Research Letters* (2016) 11:269

Page 4 of 6

Fig. 4 Schematic of the cell-based model of the CF in the RS layer. *N* is the number of slices (CF length) of the most constrictive part of the CF and *n* is the number of cells in each slice (CF width)

where $n = R_0/R_{on}$, R_0 is the resistance value of a single CF path with one chain of cells and k is a parameter related to the defect generation and diffusion [33]. The Weibull slope proportional to n, i.e., $1/R_{on}$ in Eq. (1), indicates that under the thermal dissolution effect [34], defects in the cells have diffused out and the constrictive part of the CF has changed before the reset point. Thus, according to the model, the change of Weibull slopes of V_{reset} and I_{reset} distributions as a function of R_{on} in the Cu/HfO$_2$/Pt RRAM device in this work indicates that the microstructure of the CF has degraded under the thermal dissolution effect. In a previous study [34], the Weibull slopes of the switching parameters independent of the initial resistance state indicate that the reset point corresponds to the initial step in CF dissolution. The abrupt or gradual reset transition is closely related to the initial CF resistance (R_{on}), according to the thermal dissolution mechanism [35], which can be influenced by the current compliance during the measurement. The drastic dissolution of the CF may be attributed to a great deal of Joule heat produced in the stronger CF with lower R_{on} and the heat loss along the CF [35]. The analytical cell-based reset model can provide an inspiration for the analysis of what has happened in the CF of Cu/HfO$_2$/Pt RRAM before the reset point.

To better interpret and simulate the experimental reset statistics of the Cu/HfO$_2$/Pt device, a Monte Carlo simulator has been established based on the proposed cell-based model for the reset statistics [33]. In our simulation, V_{reset} is assumed as to present an arbitrary Weibull distribution and is assumed as expressed by:
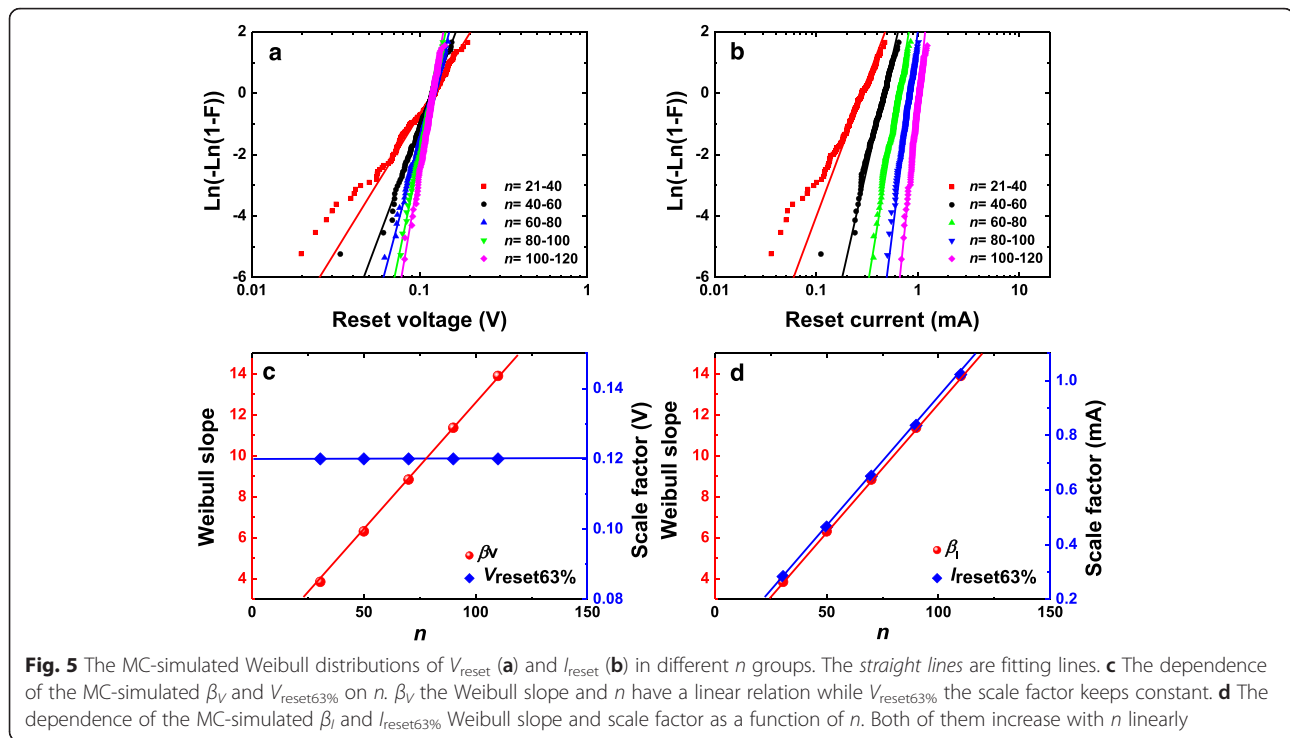
$$V_{reset} = V_{reset63\%}Ln(1-F_V)^{1/\beta_V}, \qquad (2)$$

where $F_V = r_1$, $n = n_{min} + (n_{max} - n_{min})r_2$. $V_{reset63\%}$ is the scale factor abstracted from the experimental global V_{reset} distribution and r_1 and r_2 are random numbers between 0 and 1. Using Eqs. (1) and (2), the simulated I_{reset} distributions can be obtained by:

$$I_{reset} = V_{reset}/R_{on}. \qquad (3)$$

In the simulation, we use $V_{reset\ 63\%} = 0.12$ V on the basis of the experimental result in Fig. 3a. Since R_0 represents the resistance of a single CF path with one chain of cells, we can assume $R_0 = 1/G_0$, where $G_0 = 2e^2/h$ is the quantum of conductance, as we have adopted in Ref. [36]. According to the range of R_{on} in Fig. 3, we can calculate that $n_{min} = 21$ and $n_{max} = 120$. By fitting the experimental $\beta - 1/R_{on}$ data in Fig. 3c, d with Eq. (1), $k = 0.124$ can be got. The above values are used to conduct the simulation. One thousand cycles have been constructed to match the practical number of experimental switching cycles. For each cycle, according to Eqs. (2) and (3), the simulated V_{reset} and I_{reset} values were achieved through generating random values for r_1 and r_2. Then we study the statistical distribution of the simulated V_{reset} and I_{reset} in each n group. Figure 5a, b illustrates the simulated V_{reset} and I_{reset} distributions in each n range. Figure 5c, d presents the Weibull slopes of V_{reset} and I_{reset} which have a linear correlation with n, i.e., linearly increase with or $1/R_{on}$ and the scale factor of V_{reset} is independent of R_{on} while that of I_{reset} increases with $1/R_{on}$ in linearity. The simulated results perfectly capture the experimental results. Thus, the dissolution event has finished in the CF in the reset point, which is demonstrated from both the experimental and simulation aspects.

As the abrupt reset behavior has the advantages to the reliable binary operation of RRAM, it is important to control the reset transition. Some methods can be used to get the abrupt reset switching. For example, utilizing current sweep [37, 38] operation in a single RRAM cell or using gate voltage sweep operation in a 1T1R structure [39], the reset transition can be implemented to preset well-controlled abrupt switching characteristics. By combining the above method with the approaches of increasing resistances such as introducing a barrier layer, it is expected to achieve the abrupt and low-power set/reset operation.

Zhang *et al. Nanoscale Research Letters* (2016) 11:269

Page 5 of 6

Fig. 5 The MC-simulated Weibull distributions of V_{reset} (**a**) and I_{reset} (**b**) in different n groups. The *straight lines* are fitting lines. **c** The dependence of the MC-simulated β_V and $V_{reset63\%}$ on n. β_V the Weibull slope and n have a linear relation while $V_{reset63\%}$ the scale factor keeps constant. **d** The dependence of the MC-simulated β_I and $I_{reset63\%}$ Weibull slope and scale factor as a function of n. Both of them increase with n linearly

Conclusions

The detailed microstructure evolution before the reset point in the CF of $Cu/HfO_2/Pt$ RRAM devices has been analyzed. The Weibull slopes of our device change with the different on-resistance or CF size. This result indicates that dissolution has just finished at the reset point. The obvious Joule heat generation in the wide CF may be the underlying reason for the drastic CF dissolution. To model the experimental results, a Monte Carlo simulator has been established and the simulated results are fully in consistency with those of the experiment.

Competing interests
The authors declare that they have no competing interests.

Authors' contributions
MZ and SL did the statistical data analysis. SL, JS, EM and MZ interpreted the results. MZ and SL designed the samples and carried out the RRAM fabrication. ZM and SL drafted the manuscript. YL, QL, HL, EM, JS, and ML participated in the manuscript writing and discussion of results. All authors critically read and contributed to the manuscript preparation. All authors read and approved the final manuscript.

Acknowledgments

Author details
[1]Key Laboratory of Microelectronics Devices and Integrated Technology, Institute of Microelectronics of Chinese Academy of Sciences, Beijing 100029, China. [2]Jiangsu National Synergetic Innovation Center for Advanced Materials (SICAM), Nanjing 210023, China. [3]Departament d'Enginyeria Electrònica, Universitat Autònoma de Barcelona, Bellaterra 08193, Spain.

References
1. Waser R, Dittmann R, Staikov G, Szot K (2009) Redox-based resistive switching memories–nanoionic mechanisms, prospects, and challenges. Adv Mater 21:2632–2663.
2. A Sawa (2008) Resistive switching in transition metal oxides. Mater Today 11:28-36
3. Pan F, Gao S, Chen C, Song C, Zeng F (2014) Recent progress in resistive random access memories: materials, switching mechanisms, and performance. Mater Sci Eng R 83:1–59.
4. Waser R, Aono M (2007) Nanoionics-based resistive switching memories. Nat Mater 6:833–840.
5. Wong HSP, Lee HY, Yu S, Chen YS, Wu Y, Chen PS, Lee B, Chen FT, Tsai MJ (2012) Metal–Oxide RRAM. Proc IEEE 100:1951-1970
6. Borghetti J, Snider GS, Kuekes PJ, Yang JJ, Stewart DR, Williams RS (2010) 'Memristive' switches enable 'stateful' logic operations via material implication. Nature 464:873-876
7. Kim K-H, Gaba S, Wheeler D, Cruz-Albrecht JM, Hussain T, Srinivasa N, Lu W (2011) A functional hybrid memristor crossbar-array/CMOS system for data storage and neuromorphic applications. Nano Lett 12:389–395.
8. Li Y, Xu L, Zhong Y-P, Zhou Y-X, Zhong S-J, Hu Y-Z, Chua LO, Miao X-S (2015) Associative Learning with Temporal Contiguity in a Memristive Circuit for Large-Scale Neuromorphic Networks. Adv Electron Mater 1: 1500125
9. Li Y, Zhong Y, Xu L, Zhang J, Xu X, Sun H, Miao X (2013) Ultrafast Synaptic Events in a Chalcogenide Memristor. Sci Rep 3:1619
10. Sun H, Liu Q, Li C, Long S, Lv H, Bi C, Huo Z, Li L, Liu M (2014) Direct Observation of Conversion Between Threshold Switching and Memory

Zhang *et al. Nanoscale Research Letters* (2016) 11:269

Page 6 of 6

Switching Induced by Conductive Filament Morphology. Adv Funct Mater 24:5679–5686.

11. Liu Q, Long S, Lv H, Wang W, Niu J, Huo Z, Chen J, Liu M (2010) Controllable Growth of Nanoscale Conductive Filaments in Solid-Electrolyte-Based ReRAM by Using a Metal Nanocrystal Covered Bottom Electrode. ACS Nano 4:6162–6168.

12. Yang Y, Gao P, Gaba S, Chang T, Pan X, Lu W (2012) Observation of conducting filament growth in nanoscale resistive memories. Nat Commun 3:732.

13. Yang JJ, Strukov DB, Stewart DR (2013) Memristive devices for computing. Nat Nanotechnol 8:13–24.

14. Lu Y, Gao B, Fu Y, Chen B, Liu L, Liu X, Kang J (2012) A Simplified Model for Resistive Switching of Oxide-Based Resistive Random Access Memory Devices. IEEE Electron Device Lett 33:306–308.

15. Larcher L, Puglisi FM, Pavan P, Padovani A, Vandelli L, Bersuker G (2014) A Compact Model of Program Window in HfOx RRAM Devices for Conductive Filament Characteristics Analysis. IEEE Trans Electron Devices 61:2668–2673.

16. Syu YE, Chang TC, Tsai TM, Hung YC, Chang KC, Tsai MJ, Kao MJ, Sze SM (2011) Redox Reaction Switching Mechanism in RRAM Device With Pt/CoSiOX/TiN Structure. IEEE Electron Device Lett 32:545–547.

17. Chang K-C, Tsai T-M, Chang T-C, Wu H-H, Chen J-H, Syu Y-E, Chang G-W, Chu T-J, Liu G-R, Su Y-T, Chen M-C, Pan J-H, Chen J-Y, Tung C-W, Huang H-C, Tai Y-H, Gan D-S, Sze SM (2011) Characteristics and Mechanisms of Silicon-Oxide-Based Resistance Random Access Memory. IEEE Electron Device Lett 34:399–401.

18. Bai Y, Wu H, Zhang Y, Zhang J, Qian H, Yu Z (2013) Low power W:AlOx/WOx bilayer resistive switching structure based on conductive filament formation and rupture mechanism. Appl Phys Lett 102:173503.

19. Russo U, Ielmini D, Cagli C, Lacaita AL (2009) Self-Accelerated Thermal Dissolution Model for Reset Programming in Unipolar Resistive-Switching Memory (RRAM) Devices. IEEE Trans Electron Devices 56:193–200.

20. Ielmini D, Nardi F, Cagli C (2011) Physical models of size-dependent nanofilament formation and rupture in NiO resistive switching memories. Nanotechnology 22:254022.

21. Russo U, Ielmini D, Cagli C, Lacaita AL (2009) Filament Conduction and Reset Mechanism in NiO-Based Resistive-Switching Memory (RRAM) Devices. IEEE Trans Electron Devices 56:186–192.

22. Lanza M (2014) A Review on Resistive Switching in High-k Dielectrics: A Nanoscale Point of View Using Conductive Atomic Force Microscope. Materials 7:2155–2182.

23. Lanza M, Iglesias V, Porti M, Nafría M, Aymerich X (2011) Polycrystallization effects on the nanoscale electrical properties of high-k dielectrics. Nanoscale Res Lett 6:108.

24. Pirrotta O, Larcher L, Lanza M, Padovani A, Porti M, Nafria M, Bersuker G (2013) Leakage current through the poly-crystalline HfO2: Trap densities at grains and grain boundaries. J Appl Phys 114:134503.

25. Liu Q, Sun J, Lv H, Long S, Yin K, Wan N, Li Y, Sun L, Liu M (2012) eal-Time Observation on Dynamic Growth/Dissolution of Conductive Filaments in Oxide-Electrolyte-Based ReRAM. Adv Mater 24:1844

26. Yang Y, Pan F, Liu Q, Liu M, Zeng F (2009) Fully Room-Temperature-Fabricated Nonvolatile Resistive Memory for Ultrafast and High-Density Memory Application. Nano Lett 9:1636–1643.

27. Guan X, Yu S, Wong H-SP (2012) On the Switching Parameter Variation of Metal Oxide RRAM—Part II: Model Corroboration and Device Design Strategy. IEEE Trans Electron Devices 59:1183–1188.

28. Yu S, Guan X, Wong H-SP (2012) On the Switching Parameter Variation of Metal-Oxide RRAM—Part I: Physical Modeling and Simulation Methodology. IEEE Trans Electron Devices 59:1172–1182.

29. Li Q, Khiat A, Salaoru I, Xu H, Prodromakis T (2014) Stochastic switching of TiO2-based memristive devices with identical initial memory states. Nanoscale Res Lett 9:293.

30. Raghavan N, Pey KL, Wu X, Wenhu L, Bosman M (2012) Percolative Model and Thermodynamic Analysis of Oxygen-Ion-Mediated Resistive Switching. IEEE Electron Device Lett 33:712–714.

31. Suñé J, Tous S, Wu EY (2009) Analytical Cell-Based Model for the Breakdown Statistics of Multilayer Insulator Stacks. IEEE Electron Device Lett 30:1359–1361.

32. Luo W-C, Liu J-C, Lin Y-C, Lo C-L, Huang J-J, Lin K-L, Hou T-H (2013) Statistical Model and Rapid Prediction of RRAM SET Speed–Disturb Dilemma. IEEE Trans Electron Devices 60:3760–3766.

33. Long S, Cagli C, Ielmini D, Liu M, Suñé J (2011) Reset Statistics of NiO-Based Resistive Switching Memories. IEEE Electron Device Lett 32:1570–1572.

34. Long S, Lian X, Ye T, Cagli C, Perniola L, Miranda E, Liu M, Suñé J (2013) Cycle-to-Cycle Intrinsic RESET Statistics in HfO2-Based Unipolar RRAM Devices. IEEE Electron Device Lett 34:623–625.

35. Long S, Perniola L, Cagli C, Buckley J, Lian X, Miranda E, Pan F, Liu M, Suñé J (2013) Voltage and Power-Controlled Regimes in the Progressive Unipolar RESET Transition of HfO2-Based RRAM. Sci Rep 3:2929.

36. Long S, Lian X, Cagli C, Perniola L, Miranda E, Liu M, Suñé J (2013) A Model for the Set Statistics of RRAM Inspired in the Percolation Model of Oxide Breakdown. IEEE Electron Device Lett 34:999–1001.

37. Lian W, Lv H, Liu Q, Long S, Wang W, Wang Y, Li Y, Zhang S, Dai Y, Chen J, Liu M (2011) Improved Resistive Switching Uniformity in Cu/HfO2/Pt Devices by Using Current Sweeping Mode. IEEE Electron Device Lett 32: 1053-1055

38. Wang G, Long S, Yu Z, Zhang M, Li Y, Xu D, Lv H, Liu Q, Yan X, Wang M, Xu X, Liu H, Yang B, Liu M (2015) Impact of program/erase operation on the performances of oxide-based resistive switching memory. Nanoscale Res Lett 10:39.

39. Liu H, Lv H, Yang B, Xu X, Liu R, Liu Q, Long S, Liu M (2014) Uniformity Improvement in 1T1R RRAM With Gate Voltage Ramp Programming. IEEE Electron Device Lett 35:1224–1226.